Time-frequency Characteristics Clustering of Metallic Plume during High Power Disk Laser Welding

X. D. Gao, R. L. Wang, and Y. C. Yang

Abstract—Metallic plume is an important phenomenon during high power disk laser deep-penetration welding, which can reflect the welding quality. To study this laser-induced plume characteristics and its relation to welding quality, an extraviolet and visible sensitive high speed color camera was used to capture the metallic plumes in a high-power disk laser bead on plate deep-penetration welding of Type 304 austenitic stainless steel plates at a continuous laser power of 10 kW. These captured digital images were transfered to the HSI (Hue-Saturation-Intensity) color spaces from the RGB color spaces. The area of metallic plume was segmented and defined as the plume eigenvalue. The fluctuation of weld bead width was used to evaluate the welding stability. To monitor the plume behavior, a short-time Fourier transform was applied to obtain the time-frequency characteristics of plume images. Also, the hierarchical clustering was analyzed for the time-frequency characteristics of plume images. Welding experimental results showed there existed relationship between the metallic plume and welding quality, and the fitting curve of clustering could reflect the fluctuation trend of the weld bead width effectively.

Index Terms—Disk laser welding; Metallic plume; Short-time Fourier transform; Time-frequency analysis; Hierarchical clustering

I. INTRODUCTION

High power disk laser welding is a competitive welding method and is well known for its high welding speed, good welding quality and deep penetration. In recent years, the disk laser welding has been widely used in automotive production and electronic industry. During a high power disk laser welding, a metallic plume mixture is generated quickly from the surface of the welded material. This plume mainly consists of the metal vapor and is one of the most important phenomenon which can be used to monitor the laser welding quality. Research works have shown that the metallic plume has negative effects on the energy transference efficiency of the laser beam and the welding quality [1],[2]. There exists an internal relationship between the plume characteristics and the welding status. To monitor and control the welding quality in real-time, it is necessary to investigate the metallic plume characteristics.

In recent years, some researches such as spectroscopy, photoelectric signal processing, acoustic signal processing, vision methods, and so on were performed to study the dynamic behaviors of the metallic plume [3-6]. The holographic interferometry was applied to study the laser-induced plume [7]. The Fourier transform was used to analyze the acoustic signal of metal vapor and the time-frequency was applied to study the plasma characteristics [8],[9]. These study results showed that the density and the size of the plasma were related to the laser power and beam focus position. There was a certain relations between the metallic plume and the weld quality. However, it is still difficult to find the exact relationship between the characteristics of metallic plume and the weld quality.

In order to obtain more detailed dynamic information about metallic plume, we used the high-speed photography to record the color images of metallic plume in a high power disk laser welding process. High-speed photography is an effective method and is widely used in welding measurement, it can accurately capture and monitor the metallic plume information. The important characteristic features of plumes could be extracted from these color images [10,11]. Usually, the more energy a weldment absorbs, the bigger the metallic plume is. Here, the area of metallic plume was used as the characteristic parameter and the short-time Fourier transform was applied to obtain the time-frequency characteristics of plume. Also, the hierarchical clustering was used to analyze the plume characteristics and finally a clustering curve was plotted. Welding experimental results showed that in a definite parameter combination, the 6th fitting curve of the metallic plume frequency characteristic clustering could effectively reflect the fluctuation trend of the weld bead width.

II. EXPERIMENTAL APPARATUS AND CHARACTERISTIC EXTRACTION

A. Experimental Apparatus

The schematic of a disk laser welding experimental apparatus is shown in Fig. 1. The experimental system consisted of a TruDisk-10003 disk laser welding equipment (laser power 10kW), a Motoman 6-axis robot and a welding experimental platform equipped with shielding gas (argon), servo motors and fixing devices. An extraviolet and visible

sensitive high speed color camera was used to capture the metallic plume dynamic color images during a 10kW high-power bead-on-plate disk laser welding. The welding conditions are listed in Table I.
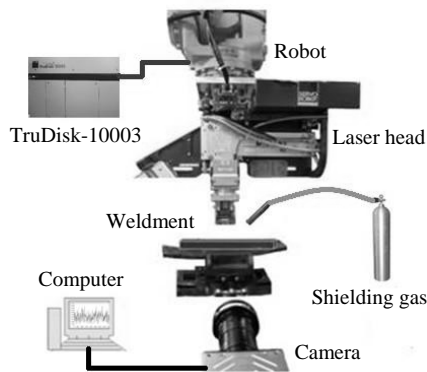

Fig. 1. Experimental apparatus of high power disk laser welding

TABLE I
WELDING EXPERIMENTAL CONDITIONS

Welding apparatus	TruDisk-10003
Laser power	10kW
Spot diameter	480μm
Laser wavelength	1030nm
Welding speed	4.5m/min
Camera speed	2000 frame/second
Image resolution	512×512 pixel
Size of weldment	150×100×10 mm
Weldment	Type 304 austenitic stainless steel

B. Extraction of Plume Characteristics

The high-speed camera collected 2400 frames RGB image of the metallic plume within 1.2 seconds, and each frame image corresponded to a welding status. The surface of a welded specimen is shown in Fig. 2. It can be seen that the middle part of the weld seam is narrow and has poor quality. This region corresponded to 1066-1333 frame images. The captured plume images from 481 to 2400 frames were processed to study their characteristics.
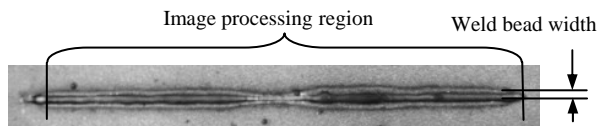

Fig. 2. Surface of a welded specimen of high-power disk laser welding

When the disk laser beam focused on a weldment, the laser energy was transfered to the surface of weldment, the weldment melted immediately and the metallic plume emerged. The area of metallic plume could reflect the absorptivity of laser energy which reflected the welding quality. Thus, the metallic plume area could be used as a characteristic parameter. In order to extract the plume characteristics accurately, the captured RGB images were converted to the HSI images. Using the image processing methods, the spatters were removed and the plume area was segmented. The image processing procedure of metallic plume is shown in Fig. 3. All plume images were processed

and the area of plume was calculated, as shown in Fig. 4. It is difficult to find there exists the obvious fluctuations of plume area. Therefore, we considered applying the methods of short-time Fourier transform and hierarchical clustering to investigate the plume characteristics.
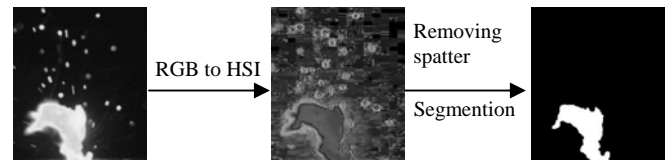

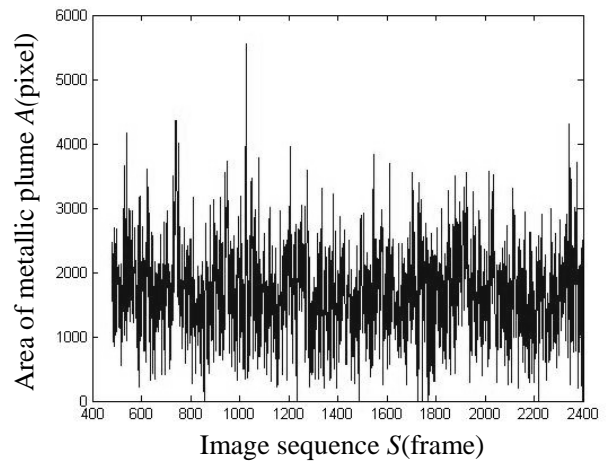Fig. 3. Schematic diagram of metallic plume image processing

Fig. 4. Curve of Metallic Plume Area with Image Sequences

III. SHORT-TIME FOURIER TRANSFORM

A. Concept of Short-time Fourier Transform

Short-time Fourier transform(STFT) can not only reflect the time-domain feature of signals, but also present the spectrum of signals clearly. Its basic idea is that the signal to be transformed is multiplied by a limited window function before the Fourier transform is applied, and this window function is nonzero for only a short period of time. This window slides along the time axis, resulting in a two-dimensional representation of the signal. This can be mathematically written as [12]

$$\text{STFT}_Z(t, f) = \int_{-\infty}^{\infty} z(t)\eta^*(t - t')e^{-j2\pi ft}dt \qquad (1)$$

where $z(t)$ is the signal to be transformed and $\eta^*(t - t')$ is the window function around t'. Through $z(t)\eta^*(t - t')$, the signal around t' is obtained and the short-time Fourier transform is just the Fourier transform of $z(t)\eta^*(t - t')$.

B. Window Function

The frequently-used window functions are Rectangular window, Gauss window, Hanning window, Hamming window, Blackman window, Triangle window, Cosine slope window, Index window and Bartlett-Hanning window. In welding experiment, Gauss window, Hanning window, Hamming window and Bartlett-Hanning window were applied to the short-time Fourier transform.

Suppose $x(n)$ is the signal sequence and $w(n)$ is a window function whose length is N. The expression of the Gauss window is

$$w(n) = e^{-\frac{1}{2}(\frac{n-(N-1)/2}{\sigma(N-1)/2})^2} \qquad (2)$$

where $\sigma \le 0.5$.

The expression of the Hanning window is

$$w(n) = 0.5 - \left(1 - \cos\left(\frac{2\pi n}{N-1}\right)\right) \qquad (3)$$

The expression of the Hamming window is

$$w(n) = 0.53 - 0.46\cos\left(\frac{2\pi n}{N-1}\right) \qquad (4)$$

The expression of the Bartlett-Hanning window is

$$w(n) = 0.42 - 0.5\cos\left(\frac{2\pi n}{N-1}\right) + 0.08\cos\left(\frac{4\pi n}{N-1}\right) \qquad (5)$$

In order to improve the temporal resolution of short-time Fourier transform, the length of window function should be as short as possible. At the same time, in order to get a higher frequency resolution, the length of the window should be as long as possible. In practical application, the length of the window function should be adapted to the length of signal local smooth length [13]. In laser welding experiment, the numerical values of length were set to be 64, 128, 256, respectively.

C. Analysis of Short-time Fourier Transform

In short-time Fourier transform, the different window types, different window length and different step length were chosen. The detailed combination parameters are listed in Table II.

TABLE II
COMBINATION PARAMETERS OF SHORT-TIME FOURIER
TRANSFORM

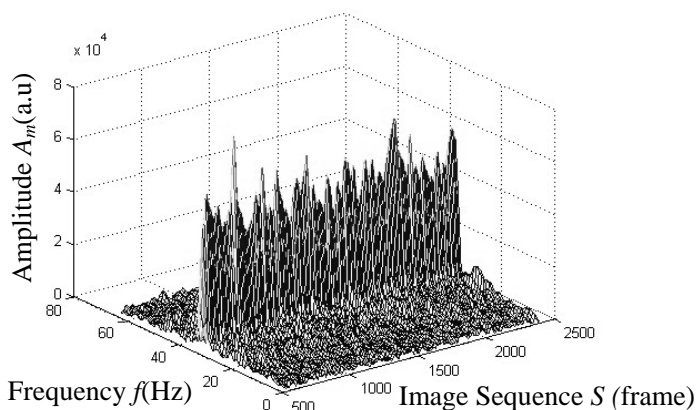| Window types	Gauss, Hanning, Hamming, Bartlett-Hanning
Length	64, 128, 256
Step length	1, 5, 10

Fig. 5. 3-D Map of time-frequency of plume area

Using the short-time Fourier transform, $4 \times 3 \times 3 = 36$ groups of data were obtained, in which the numbers of window types,

length, step length were 4, 3, 3, respectively. Taking a group of data for example, the parameters were Gauss, 64, 10. The window length was 64 and it slid along the time axis 186 times during the short-time Fourier transform, so this group of data was a matrix whose size was 64×186. Fig. 5 is a 3-D map of time-frequency information and Fig. 6 is the contour map of time-frequency.
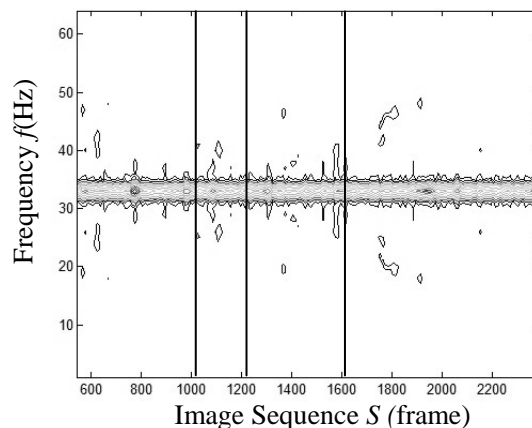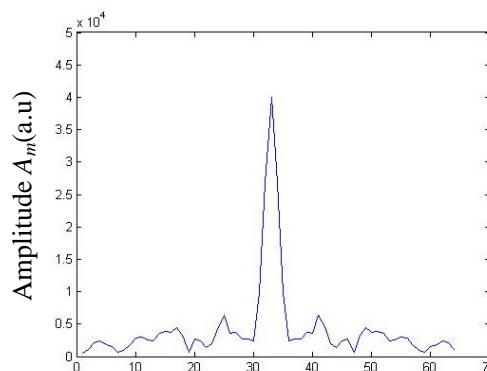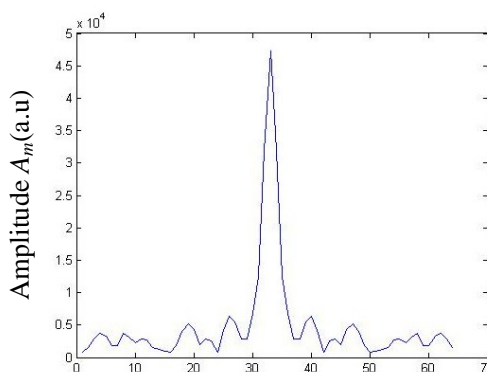

Fig. 6. Contour map of time-frequency of plume area

As mentioned above, the image sequence 1066-1333 frames corresponded to the middle part of the weld bead. This region of weld bead was narrow and had poor quality. Observing Fig. 5 and Fig. 6, there were not obvious characteristics of 1066-1333 frames. For further study, the 50th,70th,110th frequency curves were extracted to analyze their characteristics. These three groups of data corresponded to three vertical lines, shown in Fig. 6. Fig. 7 shows these three frequency curves.

(a) The 50th group of data

(b) The 70th group of data
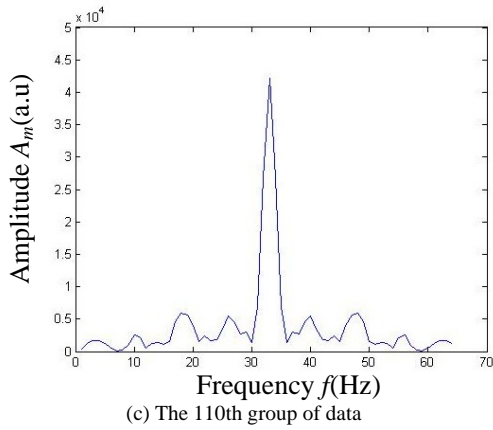
(c) The 110th group of data

Fig. 7. Curves of the 50th, 70th, 110th frequency of plume area signals

To distinguish these three frequency curves more effectively, their numerical values of average, maximum, minimum, range, interquartile range(IQR), standard deviation and sum were calculated. The range was what the biggest number minus the smallest number. The IQR is the distance between the 75th percentile and the 25th percentile. The expression of standard deviation is

$$s = \left(\frac{1}{n-1} \sum_{i=1}^{n} (x_i - \overline{x})^2 \right)^{\frac{1}{2}} \quad i=1,2,3\ldots n \qquad (6)$$

where $\overline{x}$ is the average value. All these eigenvalues are listed in Table Ⅲ.

TABLE Ⅲ
EIGENVALUES OF DIFFERENT CURVES AMONG Fig.7 (Unit: a.u)

	Fig.7 (a)	Fig.7 (b)	Fig.7 (c)
Max value	39922	47275	42242
Min value	573	815	107
Average	4199	4840	3787
IQR	1893	2318	2825
Range	39348	46459	42134
Standard deviation	6435	7702	6743
Sum	268750	309800	242410

It was found from Fig.7 that three frequency curves had similar shapes. These three curves could be distinguished from Table Ⅲ effectively by seven eigenvalues. Thus, these seven eigenvalues could represent different spectrum curves at any time. Also, we used the statistical method to calculate all frequency curve eigenvalues and analyze them by the Hierarchical clustering.

IV. HIERARCHICAL CLUSTERING

With the development of multivariate statistic analysis, the clustering analysis method has been mature gradually and widely used in Biology, Economics, Sociology, Demography and so on. The hierarchical clustering is the most important method in clustering analysis. Its basic principle is that the two closest observations are joined to create a node by calculating the distance or similar coefficient between two observations. Subsequent nodes are created by pairwise joining of observations or nodes based on the distance between them, until all the nodes merge into a desired number of clusters. At the end, a tree structure can be created by retracing which items and nodes are merged [14].

In order to decide which clusters should be combined or where a cluster should be split, a measurement of dissimilarity between sets of observations is required. In most methods of hierarchical clustering, this can be achieved by using an appropriate metric (a measure of distance between pairs of observations) and a linkage criterion which specifies the dissimilarity of sets as a function of the pairwise distances of observations.

Some commonly used distance metrics for hierarchical clustering are the Euclid distance, Minkowski distance, City Block distance, Chebyshev distance, Mahal distance, Lance distance and Cosine similarity. The linkage criteria determines the distance between sets of observations as a function of the pairwise distances between observations. There are a variety of linkage criteria between clusters. Among them, three most popular ones are maximum or complete linkage, minimum or single linkage, mean or average linkage [15]. In our welding experiments, we defined the Euclid distance and the City Block distance as the distance metrics and took minimum linkage for hierarchical clustering. The expression of Euclid distance is

$$d_{ij}^{(2)} = \left(\sum_{t=1}^{p} \left| x_{it} - x_{jt} \right|^2 \right)^{\frac{1}{2}} \qquad (7)$$

The expression of City Block distance is

$$d_{ij} = \left(\sum_{t=1}^{p} \left| x_{it} - x_{jt} \right| \right) \qquad (8)$$

Mathematically, the minimum linkage is written as

$$D_{pq} = \min(d_{ij}) \quad x_i \in G_p 、 \quad x_j \in G_q \qquad (9)$$

After the short-time Fourier transform, there were 36 groups of time frequency test data. The statistics method was used to extract the seven defined eigenvalues, then these eigenvalues were studied by clustering. The procedure of hierarchical clustering is as follows. First, the Euclid distance and the City Block distance were defined as the distance metrics, and the distance between observations were calculated. Second, the minimum linkage was used to create a tree structure. Finally, the discontinuous coefficients was set and the clustering tree was output. In this experiment, the discontinuous coefficients were 0.5, 0.7 and 0.9, respectively.
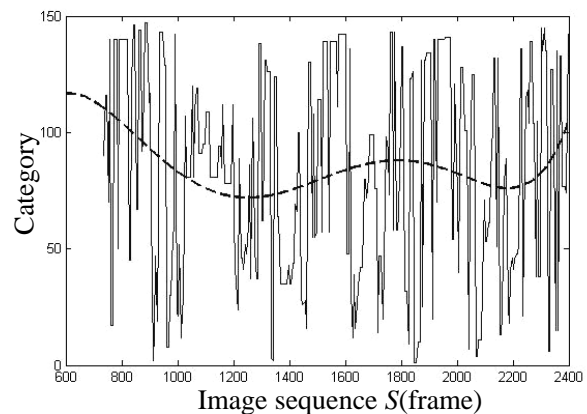

Fig. 8. Fitting curve of time-frequency clustering of metallic plume area

Totally $36 \times 2 \times 3 = 216$ groups of clustering data were

obtained after calculation. The characteristics of clustering data was analyzed by drawing the clustering curves and curve-fittings. Using Bartlett-Hanning window whose length was 256 and step value was 5 for the short-time Fourier transform, and the Euclid distance, minimum linkage and discontinuous coefficient 0.9 for hierarchical cluster, it was found that the fluctuation trend of 6th fitting of clustering curve was similar to the 6th fitting curve of weld seam bead width. That means the 6th fitting of the clustering curve could reflect the weld bead width changing trend effectively. Fig. 8 is the clustering curve based on the combination parameters mentioned above, the dotted line is the 6th fitting curve of clustering curve.

Fig. 9 shows a 6th fitting curve of the clustering curve contrasting to the 6th fitting curve of weld seam bead. In Fig. 9, the dotted line is the weld bead width, the dot and dash line is the 6th fitting curve of weld bead width and the solid line is the 6th fitting curve of the clustering curve. It can be seen that the solid line and the dot and dash line have the consistent fluctuations. The 6th fitting curve of the clustering curve could reflect the weld bead width change trend effectively. Experimental results have shown that the weld bead width can be evaluated by using the time-frequency clustering of metallic plume area. It has provided a method to monitor and evaluate the welding quality in real time during disk laser welding by analyzing the time-frequency clustering of metallic plume area.
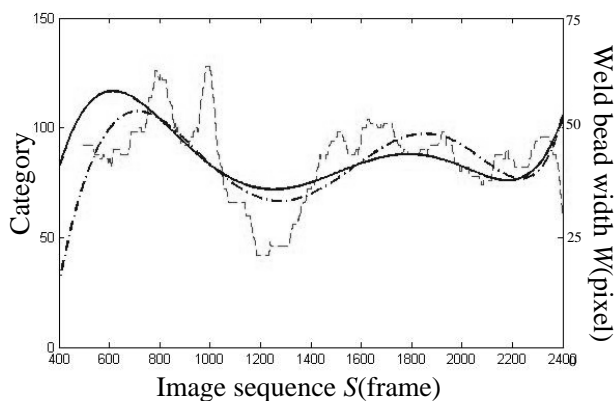

Fig. 9. Description of time-frequency clustering of metallic plume area and weld bead width

V. CONCLUSIONS

In a high power disk laser welding process, there exists a relation between the metallic plume area and the weld bead width. The metallic plume area could be calculated by using image processing techniques. It was found that the accurate plume area could be obtained by processing the plume images in the HSI color space.

The short-time Fourier transform could be applied to analyze the characteristics of plume area and extract the eigenvalues for the hierarchical clustering. Using the Bartlett-Hanning window whose length was 256 and step value was 5 for the short-time Fourier transform, and the Euclid distance, minimum linkage and discontinuous coefficient 0.9 for the hierarchical clustering, the 6th fitting curve of the clustering curve and the 6th fitting curve of weld bead width had the similar fluctuations. The 6th fitting of the

clustering curve could reflect the weld bead width changing trend effectively. Experimental results showed that the time-frequency clustering of metallic plume area could be used to monitor and evaluate the welding quality during high power disk laser welding.

REFERENCES

[1] M.M.A Khan, L.Romoli, M.Fiaschi, G.Dini, and F.Sarri, "Experimental design approach to the process parameter optimization for laser welding of martensitic stainless steels in a constrained overlap configuration," *Optics & Laser Technology*, vol.43, pp.158-172, 2011.

[2] S. Katayama, Y. Kawahito, and M. Mizutani, "Elucidation of Laser Welding Phenomena and Factors Affecting Weld Penetration and Welding Defects." *Physics Procedia*, vol.5, pp.9-17. 2010.

[3] L. Liu, M. Chen. "Interactions between Laser and Arc Plasma during Laser–arc Hybrid Welding of Magnesium Alloy," *Optics and lasers in Engineering*, Vol.49, pp.1224-1231, 2011.

[4] D. You, X. Gao, S. Katayama. "Spatter Feature Recognition during High-power Disk Laser Welding," *Advanced Materials Research*, vol.314-316, pp.937-940, 2011,

[5] M.Khaleeq-ur-Rahman, K.Siraj, M.S.Rafique, K.A.Bhatti, A.Latif, H.Jamil, and M.Basit, "Laser Induced Plasma Plume Imaging and Surface Morphology of Silicon," *Nuclear Instruments and Methods in Physics Research B*, vol.267, pp.1805-1088, 2009.

[6] T.Sibillano, A.Anocona, V.Berdi, and P.M.Lugara, "Correlation Analysis in Laser Welding Plasma," *Optics Communications*, vol.251, pp.139-148, 2005.

[7] S. H. Baik, S. K. Park, C. J. Kim, S. Y. Kim, "Holographic visualization of laser-induced plume in plused laser welding," *Optics & Laser Technology,* vol.33, pp.67-70, 2001.

[8] P. Jiang, W.Z.Chen, J.Guo, and Z.L.Tian, "The FFT Analyze of the Acoustic Signal on Plasma in Laser Welding," *Laser Journal*, vol.5, pp.62-63, 2001.

[9] A.Molino, M.Martina, F.Vacca, G.Masera, A.Terreno, G.. Pasquettaz, and G.Angelo, "FPGA implementation of time-frequency analysis algorithms for laser welding monitoring," *Microprocessors and Microsystems*, vol.33, pp.179-190, 2009.

[10] G. Li, Y. Cai, and Y. WU, "Stability information in plasma image of high-power CO_2 laser welding," *Optics and lasers in Engineering*, vol.47, pp.990-994, 2009.

[11] B.Yudodibroto, M.Hermans, and Y. Hirata, "Pendant droplet oscillation during GMAW," *Science Technology Weld Joining,* vol.11, pp.308–319, 2006.

[12] X. Wang, P. Cheng, and J. Liang, "Research of STFT Time-Frequency Analysis Algorithm and Its Application in Train Vibration Analysis," *Noise and Vibration Control*, ,vol.1, pp.65-68, 2010.

[13] Z. Ge, and Z. Chen, "*MATLAB Time-frequency analysis technology and its application,*" Beijing: Posts & Telecom Press, pp.1-8, 2006.

[14] Z. Du, and F. Lin, "A hierarchical clustering algorithm for MIMD architecture," *Computational biology and Chemistry*, vol.28, pp.417-419, 2004.

[15] Q. Zhang, and Y. Zhang, "Hierarchical clustering of gene expression profiles with graphics hardware acceleration," *Pattern Recognition Letters*, vol.27, pp.676-681, 2006.